Wind loading and response of solar tracker arrays

Juan Zaracho[1,*], John Ginger[*], David Henderson[*], Korah Parackal[**]

*Cyclone Testing Station, James Cook University, Australia.
**Insurance Institute for Business & Home Safety, USA.
1 juanignacio.zaracho@jcu.edu.au

ABSTRACT

This paper presents the analysis of an axially supported plate's response to fluctuating wind loads. It details the scaling of a solar tracker aeroelastic model, describes wind tunnel testing, and analyses results within the theoretical framework of axially supported flat plates.

1. INTRODUCTION

Single Axis Tracking (SAT) systems' lightweight components are susceptible to dynamic wind effects, potentially leading to structural failure. Previous studies by Rohr et al (2015), Taylor and Brown (2020), Martínez-García et al (2021), Enshaei et al (2023) and Cárdenas-Rondón et al (2023) has revealed its potential for vortex-induced vibrations, torsional galloping, and divergence.

2. DYNAMIC RESPONSE

The response of a plate to fluctuating wind pressures will depend on the structural properties and dimensions of the plate and support system. Structures with shallow cross-sections (where the thickness, t is significantly smaller than the breadth b), and with a long span, l can experience torsional instability called torsional galloping and divergence.

The rotational motion of a plate axially-supported by a rod or tube fixed at one end, and free at the other end as shown in Figure 1, is given by $I_0 \frac{d^2\gamma}{dt^2} + c_0 \frac{d\gamma}{dt} + k_0\gamma = M(t)$. I_0 is the polar mass moment of inertia about the centre of the axis O and is given by $I_0 = (I_{t_0} + I_{p_0} + m_p {d_0}^2)$. Here, I_{t_0} is the polar moment of inertia of the rod, I_{p_0} the polar moment of inertia of the plate, m_p the mass of the plate and d_0 the distance from the centre of mass of the plate, C to the centre of the rod. $c_0 = 2I_0\zeta_0(2\pi f_0)$, is the structural damping, where ζ_0 is the structural damping ratio and f_0 the torsional natural frequency. k_0 is the torsional stiffness of the rod.

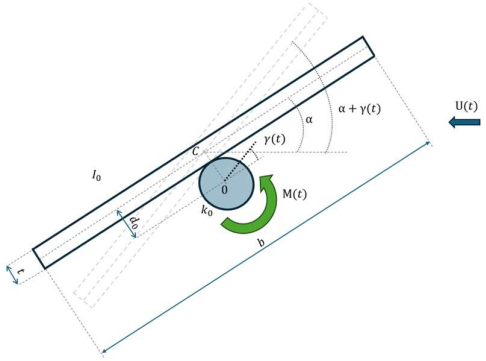

Figure 1. Torsional response of an axially-supported plate

2.1 Torsional Galloping and Divergence

Torsional galloping is a form of single degree of freedom (SDOF) structural aerodynamic instability. In torsional response, the tilt angle changes with the angle of twist, γ and with the angular velocity $d\gamma/dt$. According to Blevins (1990), for α <<< 1, the equation of motion can be expressed in the following form:

$$I_0 \frac{d^2\gamma}{dt^2} + \left(c_0 + \frac{\partial C_M}{\partial \alpha}\frac{1}{8}\rho \bar{U}_{ref} b^3 l\right)\frac{d\gamma}{dt} + \left(k_0 - \frac{\partial C_M}{\partial \alpha}\frac{1}{2}\rho {\bar{U}_{ref}}^2 b^2 l\right)\gamma = 0 \quad (1)$$

Here $\left(c_0 + \frac{\partial C_M}{\partial \alpha}\frac{1}{8}\rho \bar{U}_{ref} b^3 l\right)$ is the "effective damping" comprising structural damping, c_0 and the aerodynamic damping. The onset of torsional galloping happens when the effective damping is negative. This is only possible if $\partial C_M/\partial\alpha < 0$.

Another term of interest in Equation (*1*) is $\left(k_0 - \frac{\partial C_M}{\partial \alpha}\frac{1}{2}\rho {\bar{U}_{ref}}^2 b^2 l\right)$, the "effective stiffness". A form of instability that can be derived from that term, is called "divergence". This occurs if the sum of the structural and the aerodynamic torsional stiffness term becomes zero and is associated with tilt angles α <<< 1.

The Theodorsen's function is instrumental for analysing aeroelastic instabilities in structures like solar trackers. In the wind loading of bridges, the self-excited terms are generally represented by "aerodynamic derivatives" defined by Scanlan and Tomko (1971). Hence, the moment acting on a SAT can be described in terms of the aerodynamic derivatives as $M(t) = \frac{1}{2}\rho {\bar{U}_{ref}}^2 b^2 \left(\frac{KA_2^* b}{\bar{U}_{re}}\frac{d\gamma}{dt} + K^2 A_3^* \gamma\right) l$. Where $K = f_0 b/\bar{U}_{ref}$ is the reduced frequency of the structure. From this equation, expressions for A_2^* and A_3^* can be obtained, as shown by Taylor and Browne (2020).

$$A_2^* = -\frac{U_{red}}{4\pi}\frac{\partial C_M}{\partial \alpha} \quad \text{and} \quad A_3^* \approx \frac{1}{K^2}\frac{\partial C_M}{\partial \alpha} \quad (2)$$

$U_{red} = \bar{U}_{ref}/f_0 b$, is the reduced wind speed.

3. EXPERIMENTAL SETUP AND TESTING

3.1. Prototype and Model Scaling

The prototype system for this study is based on representative SAT types found in practice. Solar panels of breadth b = 4 m and thickness t = 40 mm are connected to frames at 1 m intervals to a l = 16 m long hollow steel torque tube with external diameter D_o = 279 mm and internal diameter D_i = 249 mm. An aeroelastic model is constructed by satisfying similarity between the model (subscript *m*) and prototype (subscript *p*) to ensure the dynamic response of the model accurately represents the prototype behaviour. The model to prototype ratio is defined by subscript r.

The Cauchy number relating inertial forces to elastic forces was matched between the model and prototype to achieve similarity with bending of the panels and torsion of the tube, as $\left(\frac{\rho\bar{U}^2}{EI/L^4}\right)_m = \left(\frac{\rho\bar{U}^2}{EI/L^4}\right)_p$ and $\left(\frac{\rho\bar{U}^2}{GJ/L^4}\right)_m = \left(\frac{\rho\bar{U}^2}{GJ/L^4}\right)_p$. Here, *EI* and *GJ* are the sectional flexural rigidity of the panels and the torsional rigidity of the torque tube. Then, given the density of the air is the same for the model and the prototype, (i.e. $\rho_r = 1$), the condition is $(EI)_r = {L_r}^4 {\bar{U}_r}^2$ and $(GJ)_r = {L_r}^4 {\bar{U}_r}^2$.

The requirement to maintain a constant ratio of inertia forces is that the density ratio of the model and the prototype must be the same: $\rho_{s_r} = 1$. This is satisfied by the mass per unit length ratio, $m_r = {L_r}^2$.

3.2. Simulated Approach Wind Flow

Tests were conducted in the 22 m long x 2 m high x 2.5 m wide open-circuit wind tunnel at the Cyclone Testing Station, James Cook University in Townsville, Australia. The approach Atmospheric Boundary Layer (ABL) was simulated to a length scale of 1/20 using a 250mm high trip board upstream end, followed by a combination of carpet and an array of blocks on the tunnel floor.

3.3. Solar Panel and Torque Tube Model

An aeroelastic model of the solar tracker array was constructed at a length scale L_r = 1/20 for a velocity ratio U_r = 1/2. The materials selected to manufacture the model were PLA plastic, for the panels and brass, for the torque tube. Given the Young's modulus of PLA (E_m = 4 Gpa), and considering a rectangular cross section, using the Cauchy number condition from section 3.1., gives thickness, t_m = 0.47 mm. Given, the mass per unit length of the prototype panel of 20 kg/m and density of PLA (= 1200 kg/m^3), results in a model mass per unit length of 0.05 kg/m. Mass was added to the model as ribs on the panels, at intervals of 50 mm, (i.e., at the edges of each individual panel).

Given the shear modulus of brass, $G_m = 36\ GPa$, the diameter of a brass rod used as the torque tube was determined with Cauchy number similarity as $D_m = 8\ mm$. The mass per unit length of model rod was 0.5 kg/m. Then, considering the density of brass (= 8800 kg/m^3), the additional mass required was added to the rod by brass screws which connected the rod to the panels. The natural frequency in torsion of the system was calculated as $f_0 = \frac{1}{2\pi}\sqrt{GJ/I_0 L}$ = 24 Hz. This value was experimentally verified by twisting the model and allowing it to freely oscillate. The moment response gave a natural frequency that closely matched the calculated frequency.

The model was supported by h = 100mm legs. A cylindrical adapter which allowed the panels to be inclined was attached to the fixed end of the rod and connected to a moment transducer (used to measure the time-varying moment M(t)), as shown in Figure 2. The model comprising sixteen modules (50 mm x 200 mm each) had a length, l = 800 mm giving an aspect ratio, l/b = 4. The brass rod was 850 mm long. The adapter and the transducer were connected at the fixed end. The panels were attached to the rod with brass screws.

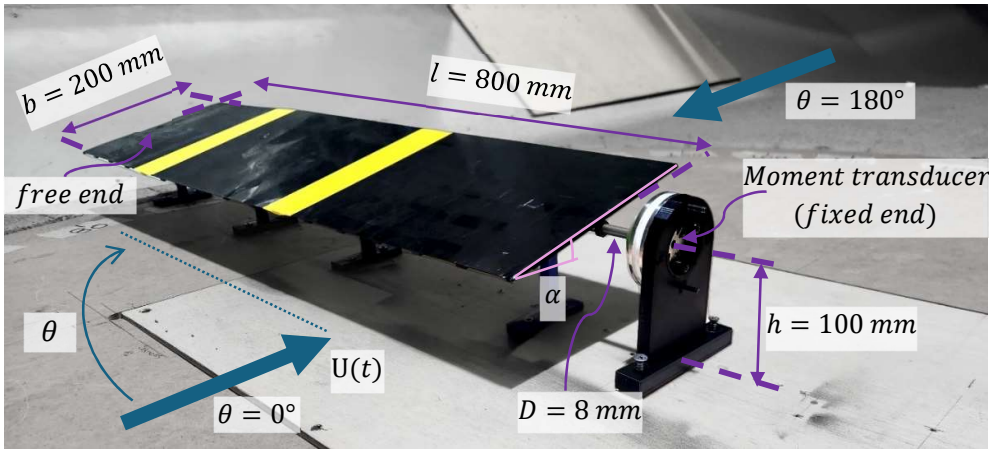

Figure 2. Solar tracking system aeroelastic model in the wind tunnel.

The model was placed on a turntable in the wind tunnel. Tests were carried out for tilt angles (α) of 0°, 5°, 10°, 20°, 25°, 30°, 40°, and 50°, and for approach wind directions (θ) 0° to 180° in increments of 10°. The time varying moment M(t) was measured at 5000 Hz and low-pass filtered at 500 Hz for 5 runs from each approach wind direction. The length and velocity ratios gave a time ratio, $T_r = L_r/U_r$ = 10. The fluctuating moments were recorded for about 60 seconds in model scale in each run, corresponding to 10 minutes in full scale. The moments measured are represented as moment coefficients referenced to the mean dynamic pressure at the tube height of 2m full-scale.

The mean, maximum and minimum, moment coefficients for each 60 second run are given by: $C_{\bar{M}} = \frac{\bar{M}_t}{\frac{1}{2}\rho \bar{U}_h{}^2 Ab}, C_{\hat{M}} = \frac{\hat{M}_t}{\frac{1}{2}\rho \bar{U}_h{}^2 Ab}, C_{\check{M}} = \frac{\check{M}_t}{\frac{1}{2}\rho \bar{U}_h{}^2 Ab}$. Here $\bar{U}_h$ is the equivalent 10-min mean wind speed at the tube height h. Wind speeds were measured by a Cobra Probe positioned at the rod height. Tests were conducted for mean wind speeds of about 3 m/s, 4.5 m/s, 5.6 m/s, 7 m/s, and 9 m/s.

4. RESULTS AND DISCUSSION

This Section presents analysis from the wind loading and dynamic response of the solar tracker model. The moment coefficients and aerodynamic derivatives are presented.

4.1. Moment Coefficient

The variation of the mean and peak C_M with wind direction for tilt angles of 0° and 20° are shown in Figure 3.

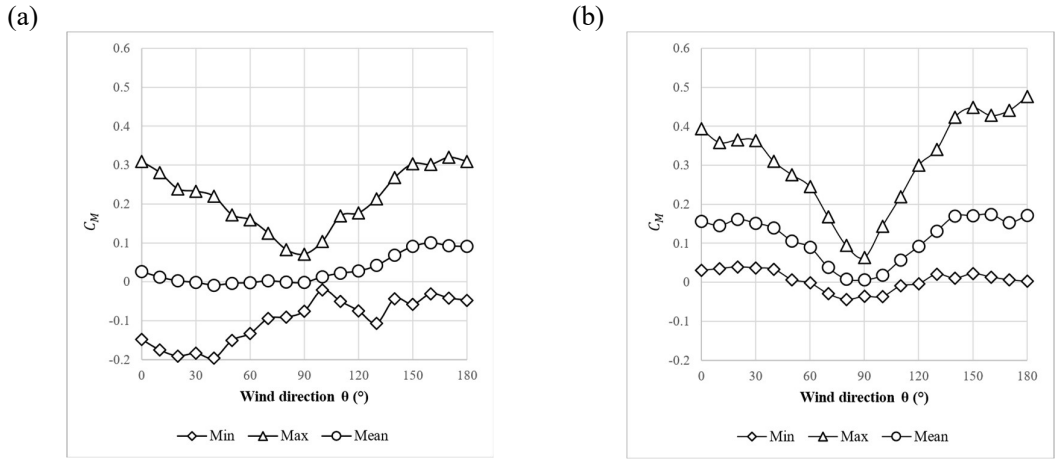

Figure 3. Maximum, mean, and minimum moment coefficients vs wind direction θ for (a) α = 0°, (b) α = 20°, at $\bar{U}_h$ = 7 m/s.

Figure 3 shows that for the case α = 0°, the mean moments are close to zero for all approach wind directions θ, with the largest peaks values at θ = 0° and 180°. The lowest peaks are observed at θ = 90° (with a mean = 0), corresponding to lateral winds. Case α = 20° shows an increase in the mean and maximum C_M, with a decrease of the minimum, which becomes positive or zero for wind directions θ closer to 0° and 180°. This indicates a prevalence in the direction of the moment acting on the system regardless the approaching direction of the wind flow. At θ = 90°, all values reduce to their minimum. Similar results were found using data from Ginger et al (2019) and by Taylor and Browne (2020) and Cárdenas-Rondón et al. (2023).

Figure 4 shows mean moment coefficients for different tilt angles α. A positive α corresponds to the wind approaching from an angle θ = 180°, and negative α corresponds to the wind approaching from θ = 0°. It can be seen that $C_{\bar{M}}$ increases for tilt angles between 0° and ±10°, reaching its peak at about ±10°. Positive tilt angles α generate higher moment coefficients than negative tilt angles.

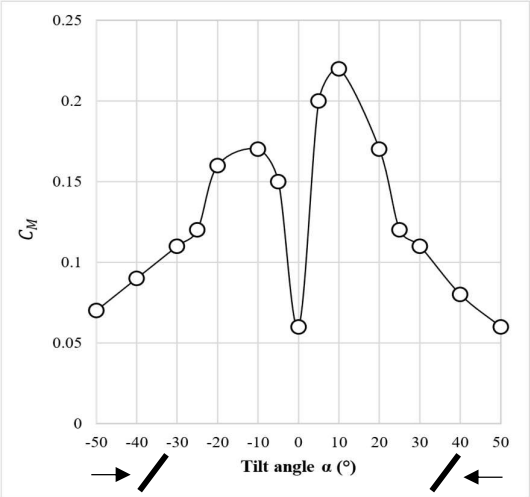

Figure 4. Mean moment coefficient vs tilt angle.

This pattern can be attributed to the position of the torque tube and the shifting centre of pressure (CP) and magnitude of the net force induced by changes in the tilt angle. For negative tilt angles, the CP is located below the tube, closer the leading edge of the plate. The resultant positive net force acts to generate a counterclockwise (i.e., positive) moment. For positive tilt angles, the CP moves above the tube. The upper surface experiences a region of large negative pressure, and resultant negative force also giving a counterclockwise moment. The decrease of the moment coefficient as the tilt angle increases both negatively and positively, could be explained by the CP locating closer to the tube as the tilt angle increases, resulting in a smaller moment.

4.2. Aerodynamic Derivatives

The aerodynamic derivatives A_2^* and A_3^* were calculated using the quasi-steady approximation of Theodorsen's functions shown in Equation (2. Figure 5 shows the derivatives as a function of the reduced wind speed, U_{red}.

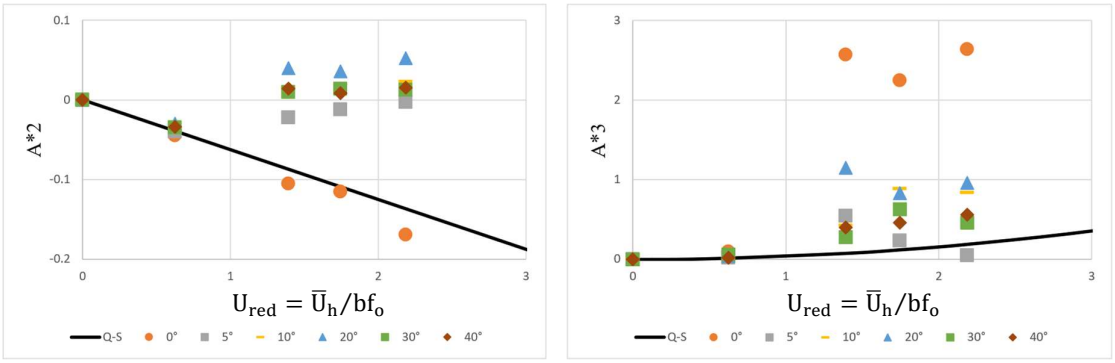

Figure 5. Aerodynamic derivatives A_2^* and A_3^*. Experimental (scatter) and quasi-steady approximation (line).

For tilt α = 0°, the derivative A_2^* tends to match the quasi-steady approximation. Yet, as the tilt increases, A_2^* values tend to zero or become slightly positive for U_{red} = 1.75 and 2.20, indicating that configurations of α = 5°, 10°, 20°, 30° and 40° are more susceptible to torsional galloping than a tilt α = 0°. This is because a positive value of aerodynamic derivative A_2^* implies a decrease of the effective damping, thus the structure is more likely to experience torsional galloping. This indicates that, for a certain structure to be stable, the mechanical damping must be increased. For α = 0°, A_2^* decreases as U_{red} increases. In agreement with Theodorsen's solution for small tilts, where a plate never reaches a positive value of A_2^*

(Theodorsen, 1935). It is observed that no positive values of A_2^* are registered before $U_{red} \approx 4$ for α = 0°, 5° and 10°.

Regarding A_3^*, although all values increase as the reduced speed increases, they do not match the quasi-steady theory. Greater values of A_3^* are observed for $\alpha = 0°$. This indicates that aerodynamic stiffness is relatively higher, thus increasing the probability of instability due to divergence.

5. CONSLUSIONS

An aeroelastic model of a single-axis solar tracker was constructed at length ratio $L_r = 1/20$ and tested in the wind tunnel to obtain moment coefficients and to evaluate the aerodynamic behaviour.

The study shows that the mean and peak moments are positive for all tilt angles between 5° and 50° and largest for $\theta = 0°$ and 180°. Negative minimums are observed for tilts between 0° and 5°. For higher tilt angles, minimums remain close to zero. An increase in the mean moment coefficient is observed for small tilt angles between 0° and 10°. A progressive decrease in the mean moment coefficient is observed as the tilt angle increases from 10° to 50°.

Torsional galloping was not observed within the tested range of wind speeds and tilt angles. Values obtained of the aerodynamic derivative A_2^* did not reduce the effective damping sufficiently to observe torsional galloping. This suggests that the structural damping may be larger than the aerodynamic damping.

Divergence was not observed at lower tilt angles. Increasing positive values of aerodynamic derivative A_3^* were obtained. Larger values corresponded to tilt $\alpha = 0°$. Nonetheless, the absence of divergence suggests that the structural stiffness may be larger than the aerodynamic stiffness.

6. REFERENCES

Blevins, R. D. (1990). *Flow-induced vibration* (K. P. Company, 2nd Ed.).

Cárdenas-Rondón, J. A., Ogueta-Gutierrez, M., Franchini, S. and Manzanares-Bercial, R. (2023). "Stability analysis of two-dimensional flat solar trackers using aerodynamic derivatives at different heights above ground". *Journal of Wind Engineering & Industrial Aerodynamics* 243.

Enshaei, P., *et al*. (2023). Low-Tilt Torsional Instability of Single-Axis Solar Trackers. 16th International Conference on Wind Engineering, Florence, Italy.

Ginger, J. D., Bodhinayake, G. G., and Ingham, S. (2019). Wind loads for designing ground-mounted solar-panel arrays. *Australian Journal of Structural Engineering*, 20(3), 204-218. https://doi.org/https://10.1080/13287982.2019.1623001

Martínez-García, E., Blanco-Marigorta, E., Parrondo Gayo, J., and Navarro-Manso, A. (2021). "Influence of inertia and aspect ratio on the torsional galloping of single-axis solar trackers." *Engineering Structures* 243.

Rohr, C., Bourke, P. A., and Banks, D. (2015). Torsional Instability of Single Axis Solar Tracking Systems Rohr Bourke Banks 2015.pdf. 14th International Conference on Wind Engineering. Porto Alegre - Brazil.

Scanlan, R. H. and Tomko, J. J. (1971). "Airfoil and bridge deck flutter derivatives". *Journal of the engineering mechanics division*. 97 (6): 1717-1737.

Taylor, Z.J. and Browne, M.T.L. (2020). "Hybrid pressure integration and buffeting analysis for multi-row wind loading in an array of single-axis trackers." *Journal of Wind Engineering & Industrial Aerodynamics* 197.

Theodorsen, T. (1935). General Theory of Aerodynamic Instability and the Mechanism of Flutter. National Advisory Committee for Aeronautics, Technical Report. 496.